

Thermodynamic non-equilibrium and anisotropy in Mars atmosphere entry

Gennaro Zuppardi*

*Department of Industrial Engineering – Aerospace Division
University of Naples “Federico II”, Piazzale Tecchio 80, 80125 Naples, Italy*

(Received April 20, 2020, Revised September 3, 2020, Accepted September 8, 2020)

Abstract. Mars exploration demands aerodynamic computations for a proper design of missions of spacecraft carrying instruments and astronauts to Mars. Both Computational Fluid Dynamics (CFD) and Direct Simulation Monte Carlo (DSMC) method play a key role for this purpose. To the author’s knowledge, the altitude separating the fields of applicability of CFD and DSMC in Mars atmosphere entry is not yet clearly defined. The limitations in using DSMC at low altitudes are due to technical limitations of the computer. The limitations in using CFD at high altitudes are due to thermodynamic non-equilibrium. Here, this problem is studied in Mars atmosphere entry, considering the Mars Pathfinder capsule in the altitude interval 40-80 km, by means of a DSMC code. Non-equilibrium is quantified by the relative differences between translational temperature and: rotational (θ_{tr}), vibrational (θ_{tv}), overall (θ_{tov}) temperatures, anisotropy is quantified by the relative difference between the translational temperature component along x and those along y (θ_{x-y}) and along z (θ_{x-z}). The results showed that θ_{tr} , θ_{tv} , θ_{x-y} , θ_{x-z} are almost equivalent. The altitude of 45 km should be the limit altitude for a proper use of a CFD code and the altitude of 40 km should be the limit altitude for a reasonable use of a DSMC code.

Keywords: thermodynamic non-equilibrium; anisotropy; Mars entry; direct simulation Monte Carlo method

1. Introduction

The forthcoming Mars exploration and colonization demand precise aerodynamic computations aimed at a proper design of the missions of spacecraft that will carry instruments and astronauts to Mars. Both Computational Fluid Dynamics (CFD) for the solution of the Navier-Stokes (NS) equations and the Direct Simulation Monte Carlo (DSMC) method play a key role for this purpose: CFD for the solution of flow fields at low altitude or in continuum, DSMC for the solution of rarefied flow fields or at high altitude. In Mars atmosphere, the altitude separating the fields of applicability of CFD and DSMC and therefore the altitude interval in which both methods work, are not yet clearly defined.

The limitations of DSMC in solving flow fields at low altitudes are due to technical limitations of the computer i.e., memory capacity and processing speed. The failure of the NS equations in simulating rarefied flow fields is due to loss of equilibrium. The NS equations rely on the

*Corresponding author, Lecturer, E-mail: zuppardi@unina.it

hypothesis that the thermal or peculiar velocity distribution function of the molecules is a small perturbation of the Maxwell distribution f_0 (Bird 1998) which was obtained in equilibrium hypothesis; f_0 is a function of thermodynamic temperature T:

$$f_0 = \frac{1}{\pi^{3/2}} \frac{1}{c^3} \exp\left(-\frac{C'^2}{c^2}\right) \quad (1)$$

being: C' the molecule thermal velocity, c the most probable molecule thermal velocity:

$$c = \sqrt{2RT} \quad (2)$$

The NS equations were obtained by the first order Chapman-Enskog expansion of a perturbation parameter ε which has to be small compared with unity (Bird 1998):

$$f = f_0(1 - \varepsilon) \quad (3)$$

ε is a function of local Knudsen numbers $Kn_{L_{u0}}$ and Kn_{L_T} and increases with them therefore with rarefaction:

$$Kn_{L_{u0}} = \frac{\lambda}{L_{u0}}, \quad Kn_{L_T} = \frac{\lambda}{L_T} \quad (4)$$

where: λ is the local mean free path, L_{u0} and L_T are the scale lengths of the macroscopic gradients of the x-component of local stream velocity (u_0) and of temperature (T) (Bird 1998), respectively:

$$L_{u0} = \frac{u_0}{\partial u_0 / \partial y}, \quad L_T = \frac{T}{\partial T / \partial y} \quad (5)$$

Mathematical processing of Eq. (3) provides “simple” equations for the computation of shear stress, heat flux and diffusion velocity of chemical species. These equations (known also as phenomenological equations) consist of the products of the gradients of stream velocity, temperature and concentration of chemical species by the related transport coefficient: viscosity μ (law of Newton), thermal conductivity K (law of Fourier), diffusivity D (law of Fick). Since ε increases with rarefaction, the Chapman-Enskog equation (Eq. (3)) breaks down with altitude and consequently also the phenomenological equations of Newton, Fourier and Fick therefore of the NS equations.

Failure of the NS equations can be due also to failure of the Maxwell equation because of: i) thermodynamic non equilibrium, thermodynamic temperature is not definable and translational (T_t), rotational (T_r) and vibrational (T_v) temperatures are different ($T_t \neq T_r \neq T_v$), ii) anisotropy, components of translational temperature in the three directions are different ($T_{tx} \neq T_{ty} \neq T_{tz}$).

Thermodynamic non-equilibrium and anisotropy are two aspects of the same problem. Both are generated in the shock wave and increase with increasing shock wave intensity. Physical process, generating non-equilibrium and anisotropy (Pham Van-Diep *et al.* 1989), (Candler and Boyd 1994), consists of the conversion of the free stream kinetic energy being primarily converted, by means of molecular collisions, to thermal energy in the direction perpendicular to the shock wave front. Thermal energy is then transferred, by subsequent collisions, to the directions parallel to the shock wave front and finally to the interior degrees of freedom (rotation and vibration) of molecules. Increasing rarefaction is synergic with the shock wave intensity in generating non-

equilibrium and anisotropy. Restoring equilibrium and isotropy occurs only by means of molecular collisions. Thus, as rarefaction increases, the collision number decreases and the flow field could restore neither equilibrium nor isotropy.

The study of the problem of non-equilibrium flows is topical and a very large number of scientific works has been recently published; see, for example, the works by Gao *et al.* (2018a, b and 2019) and by Seguin *et al.* (2018) and referenced papers. The research group made of Gao, Seguin and co-workers developed a parallel finite element solver for chemical and thermal non-equilibrium hypersonic flows. A finite-rate chemistry model and a two-temperature thermal non-equilibrium model are used to account for non-equilibrium processes. Good agreement was found with solutions available in literature.

As well known, DSMC can inherently deal with non-equilibrium flows therefore it does not suffer from need of specific computational methodologies like the NS equations do. This allowed Zuppari (2004) to easily study this problem. The flow field around a “classical” sphere-cone capsule re-entering Earth atmosphere from an interplanetary mission in the altitude interval 60-80 km was simulated by means of the DSMC code DS2G (Bird 1999).

In the present paper, the flow field around the Mars Pathfinder capsule (Braun and Manning 2006) has been simulated, during entry Mars atmosphere in the altitude interval 40-80 km, by means of the much more powerful DSMC code DS2V-4.5 64 bits (Bird 2008). The study in Mars atmosphere is even more interesting because, as well known, Mars atmosphere is less dense (Knudsen numbers are higher) and the shock waves are more intense (Mach numbers are higher) compared with those of Earth atmosphere. Non-equilibrium and anisotropy have been quantified and correlated with flow field rarefaction, evaluated by local and global Knudsen numbers and by Reynolds number downstream a normal shock wave.

2. Direct simulation Monte Carlo method and DS2V-4.5 64 bits code

It is well known that the Direct Simulation Monte Carlo (DSMC) method (Bird 1998, 2013), (Shen 2005) is currently the only available tool for the solution of rarefied flow fields from continuum low density regime (or slip flow) to free molecules regime. DSMC considers a gas as made up of discrete molecules; it is based on the kinetic theory of gases and computes the evolution of millions of simulated molecules, each one representing a large number of real molecules in the physical space, in the present computations between 6×10^9 and 5×10^{11} . Molecule-molecule collisions and molecule-surface interactions are computed. The computation domain is divided into cells, used both for selecting the colliding molecules and for sampling the macroscopic, fluid-dynamic quantities. The most important advantage of the method is that it does not suffer from numerical instabilities and does not directly rely on similarity parameters (i.e., Mach, Reynolds and Knudsen numbers). However, it is inherently unsteady and a steady solution is achieved after a sufficiently long simulation time.

The DSMC code, used in the present study, is the 2-D/axisymmetric DS2V-4.5 64 bits code (Bird 2008). This code is “sophisticated”. As widely reported in literature (Bird 2006), (Bird *et al.* 2009), (Gallis *et al.* 2009), a DSMC code is defined sophisticated if it implements computing procedures providing higher efficiency and accuracy with respect to a basic DSMC code. A sophisticated code, in fact, considers two sets of cells (collision and sampling) with the related cell adaptation and implements methods promoting “nearest neighbor” collisions. A sophisticated code automatically generates computation parameters such as numbers of cells and of simulated

molecules by the input numbers of megabytes and of the free stream number density. It uses a “radial weighting factor” routine in solving axisymmetric flow fields and provides optimal time step. Finally, the same collision pair cannot have sequential collisions.

Besides being sophisticated, DS2V-4.5 64 bits is also advanced. The user, in fact, can verify that the numbers of simulated molecules and of collision cells are adequate by means of the on line visualization of the ratio between the molecule mean collision separation (mcs) and the local mean free path (λ) in each collision cell. In addition, the code allows the user to change (or to increase), during a computation, the number of simulated molecules. The ratio mcs/λ has to be less than unity everywhere in the computation domain for an acceptable quality of the results. Bird (2006) suggests 0.2 as a limit value for an optimal quality of the results. Furthermore, the code gives the user information about the stabilization of a computation by means of the profile of the number of simulated molecules as a function of the simulated time. According to Bird (2006), the stabilization of a DSMC calculation is achieved when this profile becomes jagged and included within a band defining the standard deviation of the number of simulated molecules.

3. Basic equations

Translational, kinetic energy of a molecule (E_t [J]), due to thermal motion, reads (Bird 1998):

$$E_t = \frac{1}{2} m \bar{C}'^2 = \frac{1}{2} m (\bar{U}'^2 + \bar{V}'^2 + \bar{W}'^2) = \frac{3}{2} k T_t \quad (6)$$

being: m mass of a molecule [kg], U' , V' , W' components of C' [m/s] in the x -, y - and z -directions, a bar for average, k the Boltzmann constant [J/K], T_t [K] translational temperature. The three components of T_t read:

$$T_{tx} = \frac{m}{k} \bar{U}'^2, \quad T_{ty} = \frac{m}{k} \bar{V}'^2, \quad T_{tz} = \frac{m}{k} \bar{W}'^2 \quad (7)$$

Energies associated with rotation (E_r) and vibration (E_v) read:

$$E_r = \frac{1}{2} \xi_r k T_r, \quad E_v = \frac{1}{2} \xi_v k T_v \quad (8)$$

where ξ is the number of degrees of freedom and subscripts r and v are for rotation and vibration. Overall temperature (T_{ov}) represents the total energy of a stationary, non-equilibrium gas. T_{ov} is an average of translational, rotational and vibrational temperatures, weighted by the numbers of freedom degrees:

$$T_{ov} = \frac{3T_t + \xi_r T_r + \xi_v T_v}{3 + \xi_r + \xi_v} \quad (9)$$

From the equation of state of an ideal gas ($p = nkT$ [N/m²]), normal components of the pressure tensor read:

$$p_{xx} = nkT_{tx}, \quad p_{yy} = nkT_{ty}, \quad p_{zz} = nkT_{tz} \quad (10)$$

where: n [$1/m^3$] is the molecular number density. Eqs. (6), (7), (8) and (10), written for a simple gas, can be generalized for a mixture by including, in the averaging process, the molecular mass of each chemical species and the related molar fraction.

Since translational temperature and its x-component are prevalent, they have been considered as reference quantities in the definition of the parameters quantifying non-equilibrium and anisotropy. The relative differences between the gas macroscopic translational temperature with the macroscopic rotational and vibrational temperatures quantify non-equilibrium and, similarly, the relative differences between the macroscopic translational temperature component along x with those along y and z quantify anisotropy. Since in a non-equilibrium gas, translational temperature plays the role of thermodynamic temperature, a further non-equilibrium parameter is provided by the relative difference between T_t and T_{ov} :

$$\theta_{t-r} = \frac{T_t}{T_r} - 1, \quad \theta_{t-v} = \frac{T_t}{T_v} - 1, \quad \theta_{t-ov} = \left(\frac{T_t}{T_{ov}} - 1 \right) \quad (11a)$$

$$\theta_{x-y} = \frac{T_x}{T_y} - 1, \quad \theta_{x-z} = \frac{T_x}{T_z} \quad (11b)$$

Obviously, the higher θ the higher non-equilibrium and anisotropy. Equilibrium and isotropy, i.e., $T_t=T_r$, $T_t=T_v$, $T_t=T_{ov}$ and $T_x=T_y$, $T_x=T_z$, are defined by $\theta=0$ and the common value of temperature is the thermodynamic temperature (T).

4. Test conditions and quality of the results

Mars atmosphere, considered in the present computations, is made of 7 species (O_2 , N_2 , NO , CO , CO_2 , C , Ar) and its composition is constant with altitude. Table 1 reports both the mass fraction and the molar fraction of each chemical species. Due to dissociation reactions along an entry path, atomic oxygen and atomic nitrogen are also present. Therefore, for these calculations, Mars atmosphere is a mixture of 9 chemical species. The chemical model proposed by Bird in the version 3.3 of the DS2V code (Bird 2005) was used. This model is made of 54 reactions: 40 dissociations, 7 forward (or endothermic) exchanges, 7 reverse (or exothermic) exchanges.

Computations were carried out in the altitude interval between 40 and 80 km with a step of 5 km and relied on atmospheric parameters from the GRAM-2001 Mars model reported by Justus

Table 1 Chemical composition of Mars atmosphere

Chemical species	Mass fraction	Molar fraction
O_2	0.0013	0.00176
N_2	0.0270	0.04173
NO	0.0001	0.00014
CO	0.0007	0.00108
CO_2	0.9500	0.93399
C	0.0049	0.00396
Ar	0.0160	0.01734

Table 2 DS2V input data and aerodynamic parameters

h [km]	V_∞ [m/s]	T_∞ [K]	n_∞ [1/m³]	Ma_∞	$Kn_{\infty D}$	Re_{2D}
80	7269	135.4	1.94×10^{19}	38.1	1.36×10^{-2}	10.0
75	7269	143.3	4.08×10^{19}	37.0	6.65×10^{-3}	21.0
70	7268	146.2	8.09×10^{19}	36.7	3.38×10^{-3}	41.7
65	7264	146.8	1.56×10^{20}	36.6	1.76×10^{-3}	80.3
60	7253	142.7	3.20×10^{20}	37.0	8.47×10^{-4}	164.8
55	7226	134.9	7.13×10^{20}	37.9	3.71×10^{-4}	368.9
50	7161	133.0	1.53×10^{21}	37.9	1.72×10^{-4}	798.1
45	7024	137.6	2.99×10^{21}	36.5	8.90×10^{-5}	1587.6
40	6763	146.6	5.45×10^{21}	34.1	5.02×10^{-5}	2085.1

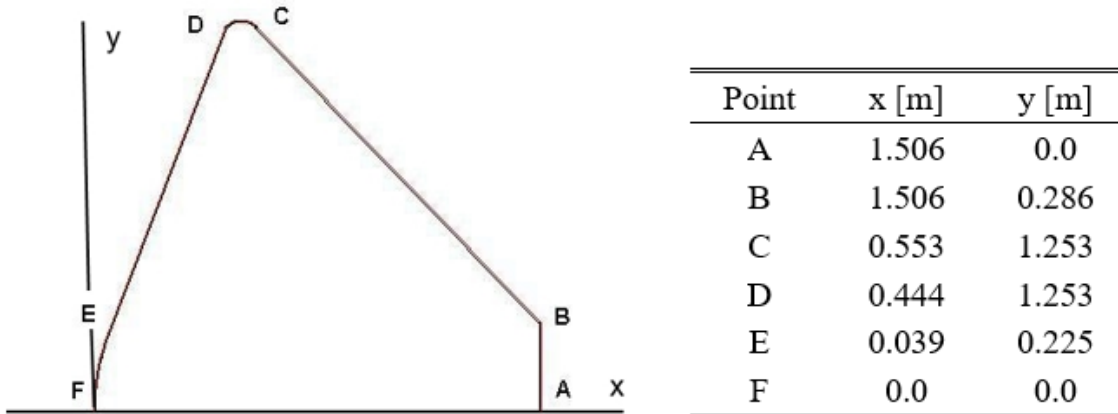


Fig. 1 Geometrical characteristics of the Mars Pathfinder capsule in the meridian plane (x, y)

and Johnson (2001). The influence of the model computing atmospheric or free stream parameters is very critical for the evaluation of every aerodynamic parameters and therefore “a fortiori” of the θ parameters. The GRAM-2001 is far more reliable than the NASA Glenn model (NASA Glenn Research Center (1996)) as verified by specific studies carried out by Zuppardi (2019a, b, 2020).

Zuppardi verified that free stream velocities (V_∞) along the two entry trajectories (or for each atmosphere model) at the altitudes of interest for this paper were equivalent: $V_\infty \cong 7260$ m/s. The most significant difference between the NASA Glenn model and the GRAM-2001 is in temperature and consequently in density. The point of greatest weakness of the Glenn model is in the linear decrease of temperature with altitude (h) for h greater than 7000 m. For example, deep space temperature (4 K) and limit temperature (0 K) would be reached at $h=110.6$ km and 112.4 km, respectively. The difference in temperature and in density strongly influences aerodynamic parameters such as free stream Mach (Ma_∞), Knudsen ($Kn_{\infty D}$) numbers and Reynolds number downstream a normal shock wave (Re_{2D}); Knudsen and Reynolds numbers are based on the Pathfinder’s diameter. For example, at $h=80$ km, $Ma_\infty=38.1$ and 51.7, $Kn_{\infty D}=1.40 \times 10^{-2}$ and 3.90×10^{-4} , $Re_{2D}=10.0$ and 267.9, for the GRAM-2001 and the NASA Glenn model, respectively. Table 2 reports input data to DS2V: free stream velocity, temperature (T_∞), number density (n_∞) as

Table 3 DS2V quality of computations

h [km]	mcs/λ	t_s/t_f
80	0.008	7.95
75	0.015	8.05
70	0.030	6.77
65	0.059	5.06
60	0.119	5.54
55	0.276	3.56
50	0.598	3.86
45	1.042	2.41
40	1.957	1.59

well as Mach, Knudsen numbers and Reynolds number downstream a normal shock wave.

Pathfinder capsule (Braun and Manning 2006) is a revolution body whose geometry, in the meridian plane (x, y), is shown in Fig. 1. The heat shield is a 70 deg cone, the nose curvature radius, i.e., the curve between points F and E, is 0.664 m and the diameter of the base area is $D=2.65$ m. The Pathfinder's entry trajectory has been computed by the integration of the equations of dynamics of the capsule (Zuppardi and Savino 2015). The capsule was considered at zero angle of attack along the whole entry path i.e. with no lift and in free entry i.e., with no thrusters and no parachute.

The evaluation of rarefaction relies both on local Knudsen numbers, such as Kn_{LV} , $Kn_{L\rho}$, Kn_{LT} and on global parameters such as Reynolds number downstream a normal shock wave (Re_{2D}) and global Knudsen number ($Kn_{\infty D}$). For the purpose of this paper, the scale length of a generic macroscopic quantity G (velocity V , density ρ and translational temperature T_t) is computed in the shock layer along the Pathfinder's stagnation line as: $L_G=G/(dG/dx)$.

According to: i) Bird (1998), the condition for the NS equations to be valid is that the local Knudsen numbers have to be less than 0.1 and the upper limit at which the continuum model has to be replaced by the molecular model is 0.2, ii) Vallerani (1973), the transitional regime for a blunt body is defined by $10^{-1}<Re_{2D}<10^4$, iii) Moss (1995), the transitional regime is defined by $10^{-3}<Kn_{\infty D}<50$. Table 2 shows that Re_{2D} and $Kn_{\infty D}$ agree in stating the flow field in transitional regime.

Table 3 verifies the quality of the results: i) the criterion by Bird for an optimal quality of a DSMC computation ($mcs/\lambda \leq 0.2$) is fully satisfied at altitudes higher than 55 km. Even though at the altitude of 40 and 45 km, mcs/λ is slightly greater than unity however the results have been included in the analysis, ii) the achievement of a steady state condition is also satisfied. In fact, as well known, a rule of thumb suggests considering an unsteady, fluid-dynamic computation stabilized when the ratio t_s/t_f is reasonably greater than unity, being t_s the simulation time and t_f the fluid-dynamic time, computed as the time necessary for the fluid to cross the length (L) of the body under study at the free stream velocity: $t_f = L/V_{\infty}$. In this case $L = 1.506$ m.

5. Analysis of the results

DS2V provides in output both mixture data, such as translational, rotational, vibrational

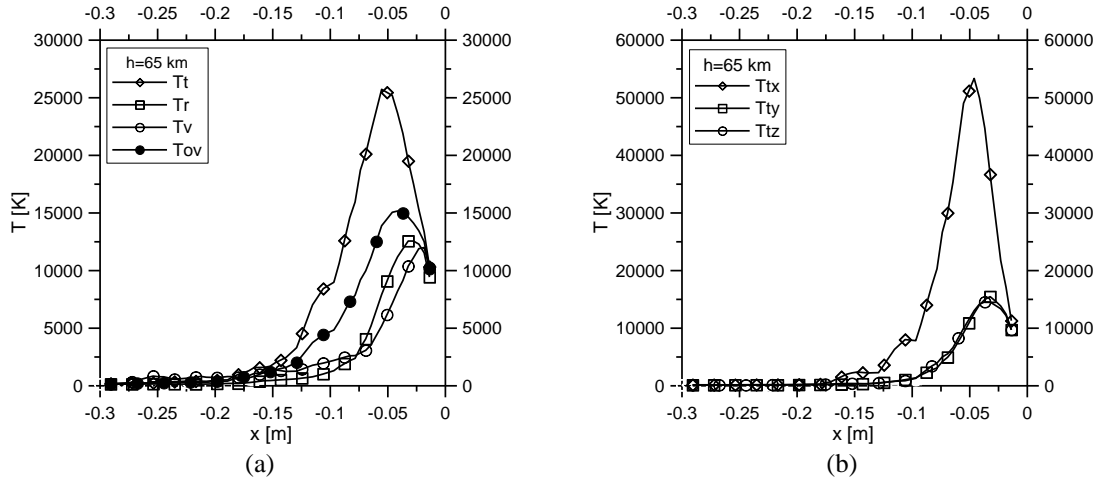


Fig. 2 Profiles of translational, rotational, vibrational and overall temperatures (a) and of the components of the translational temperature (b) along the Pathfinder's stagnation line: $h=65$ km

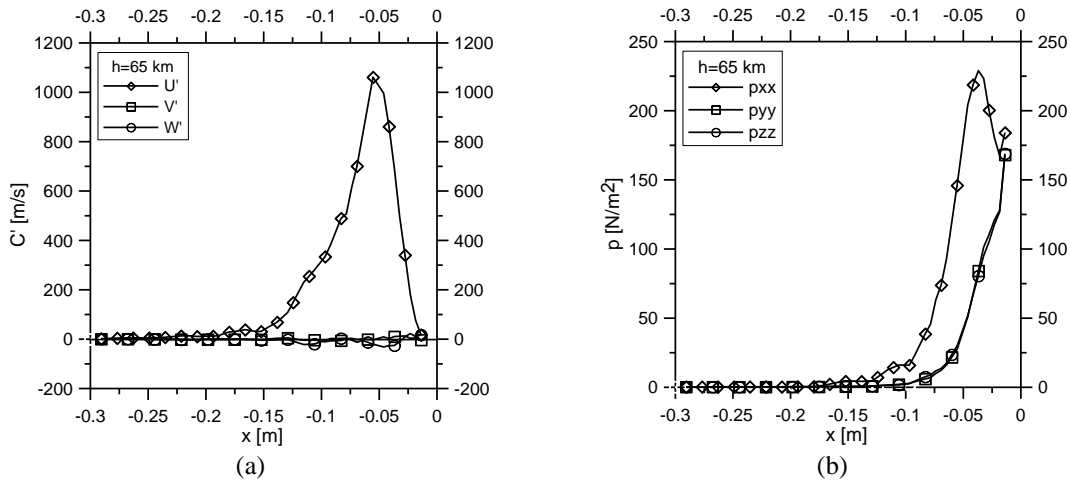


Fig. 3 Profiles of the CO_2 components of diffusion velocity (a) and of pressure (b) along the Pathfinder's stagnation line: $h=65$ km

temperatures, etc. and data for each chemical species, such as components of translational temperature, of diffusion velocity, etc.. The components of translational temperature have to be averaged over the chemical species to obtain the same quantities for the mixture. Here, data related to CO_2 have been considered as representative of those of the whole mixture. On the other hand this approximation is not very strong because, as said before, Mars atmosphere is practically made of CO_2 .

In order to provide a view or a qualitative evaluation of thermodynamic non-equilibrium and anisotropy, Figs. 2(a) and 2(b) show the profiles of translational, rotational, vibrational, overall temperature and of the components of translational temperature along the Pathfinder's stagnation line at the intermediate altitude of 65 km, respectively. Due to the link between the components of

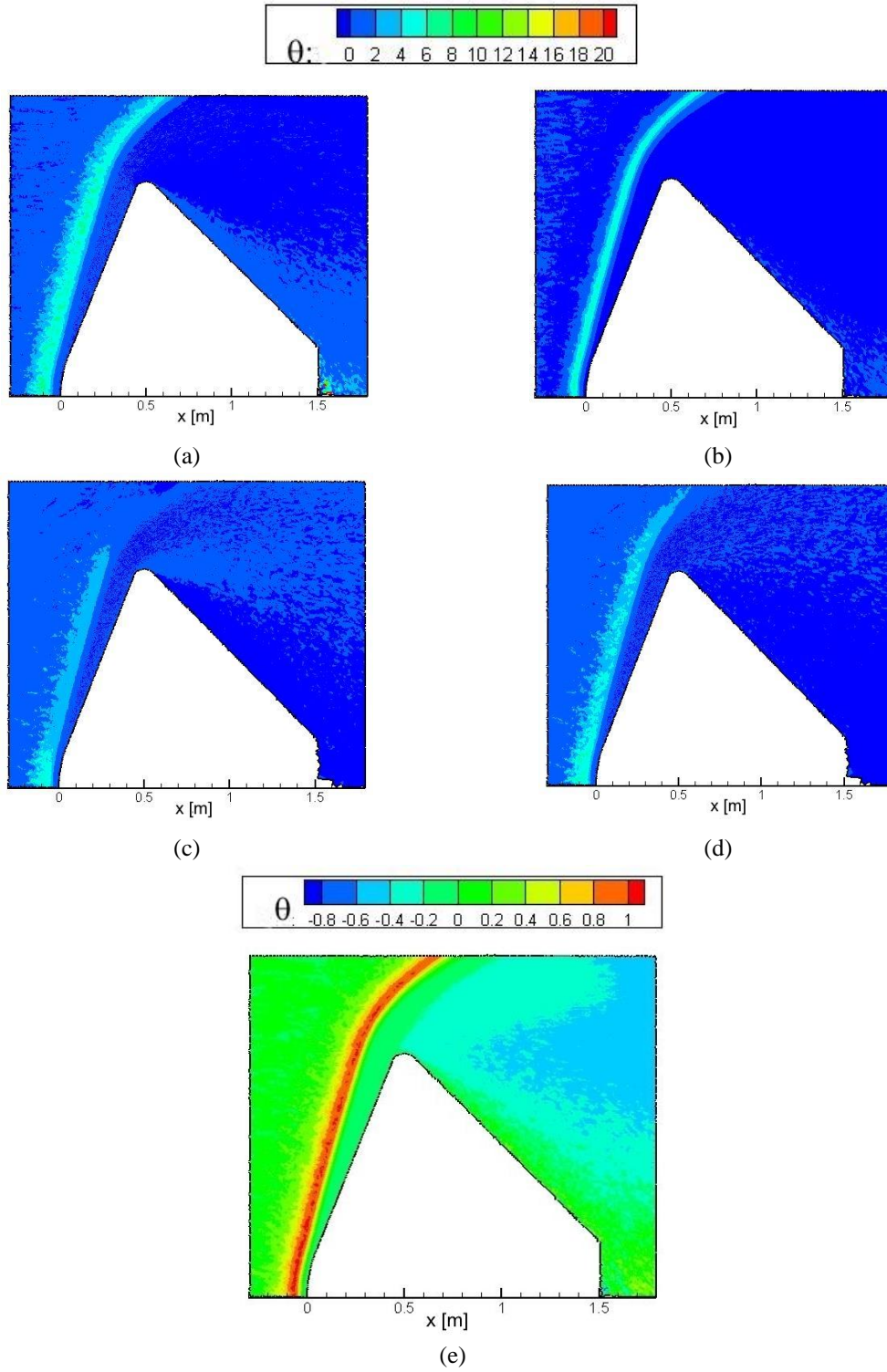


Fig. 4 2-D maps of θ_{t-r} (a), θ_{t-v} (b), θ_{x-y} (c), θ_{x-z} (d) and θ_{t-ov} (e): $h=65$ km

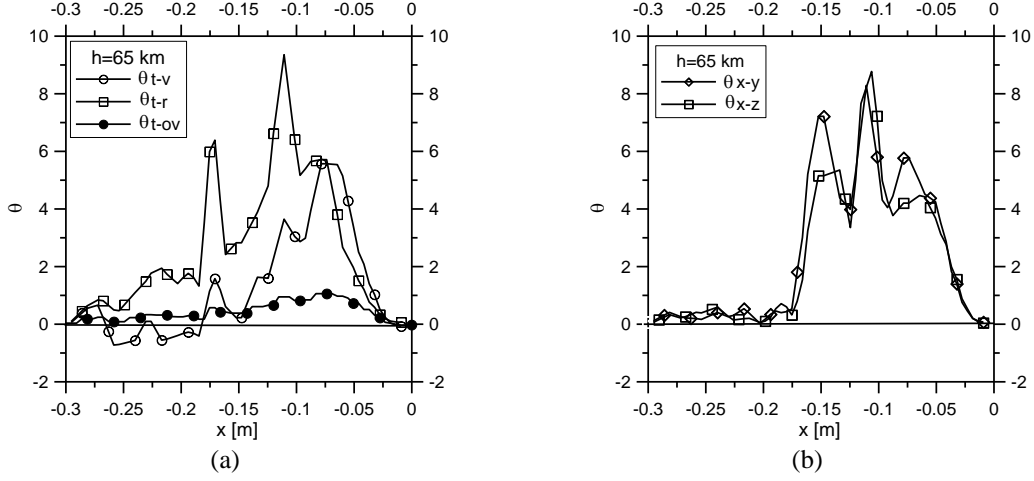


Fig. 5 Profiles of non-equilibrium (a) and anisotropy (b) parameters along the Pathfinder stagnation line: $h=65$ km

Table 4 Maximum non-equilibrium and anisotropy parameters

h [km]	$(\theta_{t-r})_{\max}$	$(\theta_{t-v})_{\max}$	$(\theta_{t-ov})_{\max}$	$(\theta_{x-y})_{\max}$	$(\theta_{x-z})_{\max}$
80	15.60	11.76	1.30	63.91	30.93
75	14.64	8.42	1.17	37.23	25.21
70	10.85	7.16	1.16	10.11	13.76
65	9.35	5.57	1.06	8.29	10.31
60	7.55	5.57	1.01	4.21	4.90
55	5.08	3.81	0.91	3.61	3.91
50	3.86	0.69	0.49	3.02	3.86
45	1.14	1.40	0.47	5.47	5.30
40	0.58	0.07	0.10	2.41	2.44

temperature and the components of diffusion velocity (Eq. (7)) and of pressure (Eq. (10)), anisotropy manifests itself also through the difference of the components of diffusion velocity and of pressure. Figs. 3(a) and 3(b) show the profiles of U' , V' , W' and of p_{xx} , p_{yy} , p_{zz} , respectively. Since, as well known, the output from any DSMC code is rather scattered, in order to improve the readability of the plots, data are represented, where ever necessary, by means of “running average” fits.

Figs. 4(a) to 4(e) show the 2-D maps of θ_{t-r} (a), θ_{t-v} (b) and θ_{x-y} (c), θ_{x-z} (d) and θ_{t-ov} at $h=65$ km. As said before, all maps show that non-equilibrium and anisotropy are concentrated in the shock wave. Figs. 5(a) and 5(b) show more in details the profiles of θ_{t-r} , θ_{t-v} , θ_{t-ov} and θ_{x-y} , θ_{x-z} along the Pathfinder’s stagnation line at $h=65$ km. Because of the axisymmetry of the flow field, the profiles of θ_{x-y} and θ_{x-z} are almost equivalent.

Both Figs. 4 and 5 clearly show that: i) maximum values of θ are got in the shock wave, ii) θ_{t-r} , θ_{t-v} , θ_{x-y} , θ_{x-z} are comparable, iii) flow is in equilibrium before and after the shock wave. The influence of altitude on non-equilibrium and anisotropy can be evaluated by means of the

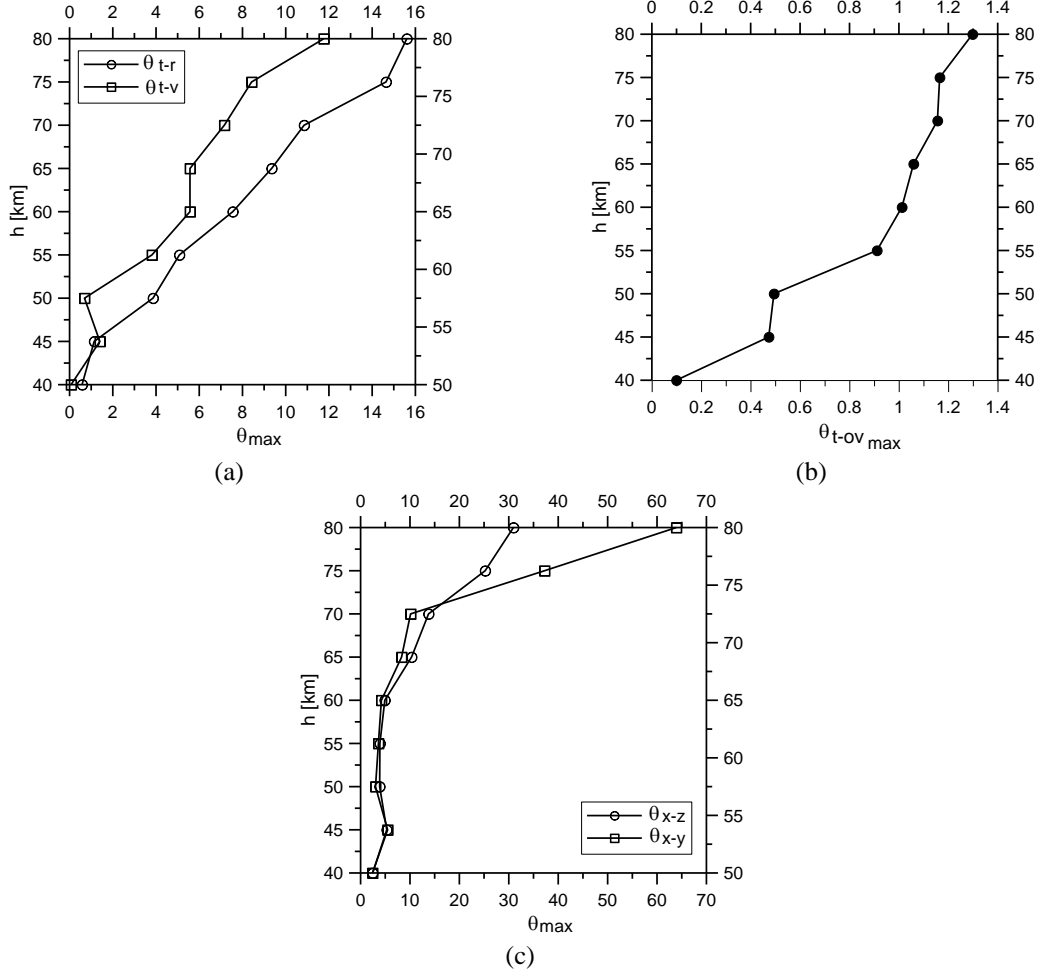


Fig. 6 Profiles of the maximum values of θ_{t-r} , θ_{t-v} (a), θ_{t-ov} (b) and θ_{x-y} , θ_{x-z} (c) as functions of altitude

maximum values of θ_{t-r} , θ_{t-v} , θ_{t-ov} , θ_{x-y} and θ_{x-z} along the stagnation line, reported in Table 4 and, for the sake of completeness, also plotted in Figs.6(a), 6(b) and 6(c). Unfortunately, due to an unknown reason, $T_{t_{max}}$ and consequently $(\theta_{t-v})_{max}$ and $(\theta_{t-ov})_{max}$ assumes at $h=50$ km a smaller value than expected. As reported in Table 4, non-equilibrium and anisotropy are equivalent up to an altitude of about 70 km where the maximum values of θ_{t-r} , θ_{t-v} , θ_{x-y} and θ_{x-z} are: 10.9, 7.2, 10.1 and 13.8, respectively. At higher altitudes, anisotropy increases dramatically (Fig. 6(c)), much more than non-equilibrium does; for example at $h=80$ km, θ_{x-y} and θ_{t-v} achieve values of 63.9 and 11.8, respectively.

As expected, non-equilibrium and anisotropy parameters increase with altitude. These increments are due both to: i) a decrease of the number of molecular collisions, quantified by the rate of molecular collisions (number of collisions per second) in the whole computation dominion (Fig. 7(a)), ii) an increase of intensity of the shock wave, quantified by the maximum value along the stagnation line at each altitude, of the translational temperature made non-dimensional by the free stream temperature (Fig. 7(b)). Figs. 7(a) and 7(b) show that, in the whole altitude interval,

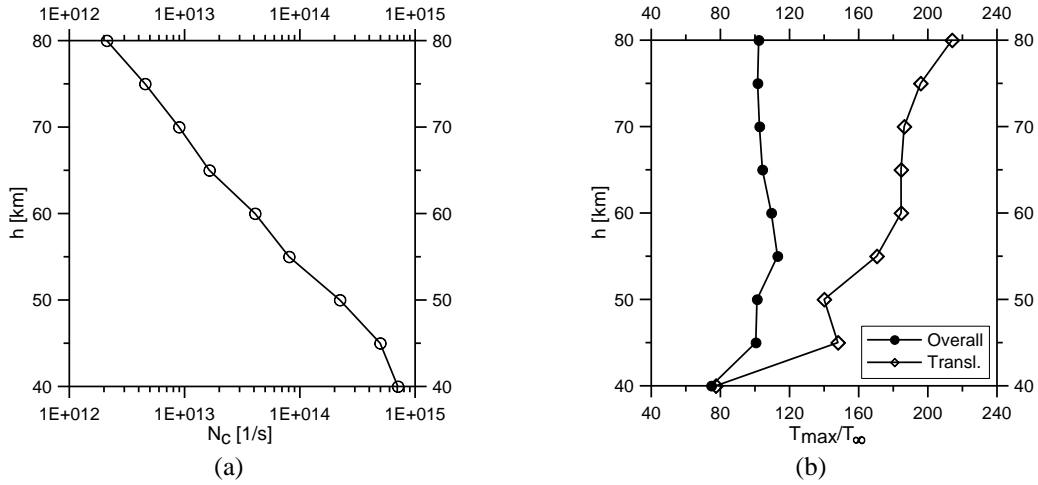


Fig. 7 Profiles of the number of collisions per second (a) and of the maximum values of translational and overall temperatures (b) as functions of altitude

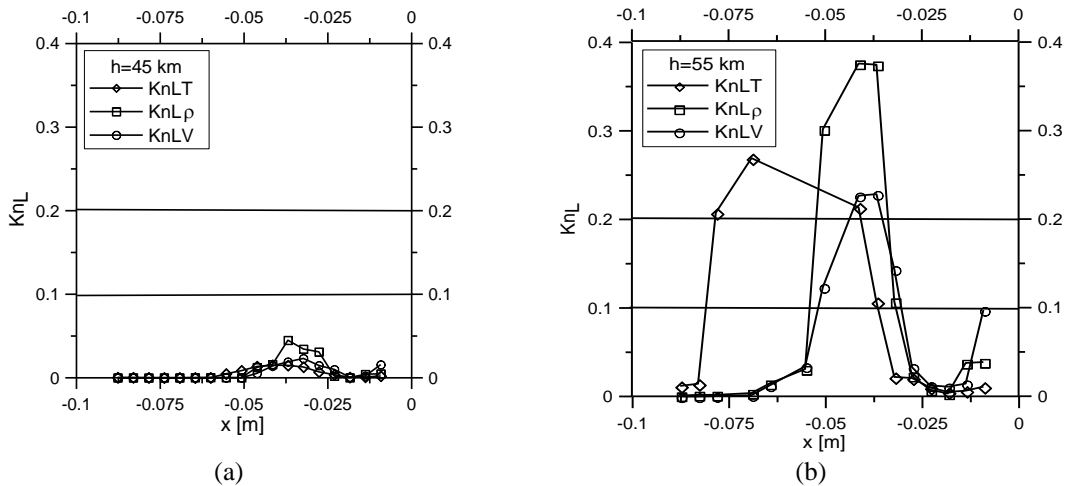


Fig. 8 Profiles of local Knudsen numbers along the Pathfinder stagnation line at $h=45$ (a) and 55 (b) km

the number of molecular collisions per second reduces of about three orders of magnitude and the shock wave intensity increases of about 177%, respectively. For the sake of completeness, the profile of the maximum values of overall temperature along the stagnation line, made non-dimensional by free stream temperature, is also shown in Fig. 7(b). The difference between the maximum values of $T_{\text{tmax}}/T_{\infty}$ and T_{ov}/T_{∞} provides a further qualitative indication of non equilibrium. As expected the difference increases with altitude; it ranges from 2.6 to 111.8 in the altitude interval.

Figs. 8(a) and 8(b) show the profiles of the local Knudsen numbers (Kn_{LT} , $Kn_{L\rho}$ and Kn_{LV}) along the stagnation line. It seems that, along Mars entry path, altitude of 45 km can be roughly considered as the limit altitude for a proper use of a NS code. In fact, the values of the local Knudsen numbers at this altitude (Fig. 8(a)) satisfy the condition of a complete validity of the NS

equations; all Knudsen numbers along the stagnation line are lower than 0.1. Correspondingly, the maximum values of θ_{t-r} , θ_{t-v} and θ_{x-y} , θ_{x-z} along the stagnation line are of the order of magnitude unitary (see Table 4). An uncertainty situation exists at $h=55$ km (Fig.8(b)). In fact, all Knudsen numbers exceed even the limit value for the assumption of continuum but the θ parameters are still of unitary order of magnitude (see Table 4).

DSMC calculation at $h=40$ km by a computer, provided with a single processor (i5, 28 GHz), required a very long time (5.38×10^5 s or 6 days and about 6 hours). Thus it can be stated that the altitude of 40 km is the lower limit altitude for a reasonable use of a DSMC code; the overlapping altitude interval, where both CFD and DSMC hold, is roughly 40-45 km.

6. Conclusions

The forthcoming Mars exploration and colonization, by means of aero-space-planes entering the Mars atmosphere and flying in it, stimulated the author to face the problem of defining the altitude limit for a proper use of a Navier-Stokes (NS) solver. The failure of the NS equations with increasing altitude is due to the failure of the Chapman-Enskog theory or of the Maxwell equation due to thermodynamic non-equilibrium (i.e., different translational, rotational and vibrational temperatures) and to anisotropy (i.e., different components in the three directions of the translational temperature). Thermodynamic non-equilibrium and anisotropy increase with increasing shock wave intensity and rarefaction.

The study has been carried out by means of a Direct Simulation Monte Carlo (DSMC) code which, as well known, can simulate non-equilibrium flow fields. Computations have been carried out by the DS2V-4.5 64 bits code, considering the entry trajectory of Mars Pathfinder in the altitude interval 40-80 km. The GRAM-2001 provided the atmosphere parameters. Non-equilibrium and anisotropy have been quantified by the relative differences of the rotational and vibrational temperatures with respect to the translational temperature and of the components of translational temperature along y and z with respect to the component along x. The relative difference between the overall temperature and the translational one has been also considered like a non-equilibrium index.

It seems that in Mars atmosphere entry, altitude of 45 km can be reasonably considered as the upper limit altitude for a safe, correct use of a NS code. This remark is also supported by a rarefaction analysis carried out in terms of local Knudsen numbers along the Pathfinder's stagnation line. The altitude of 40 km, by using a current technology computer and with single processor, can be considered as the lower altitude for a reasonable use of a DSMC code. Therefore the altitude interval, where both CFD and DSMC can be used, is roughly 40-45 km. Further tests will be carried out to state more precise correlation between rarefaction and non-equilibrium parameters, considering other spacecraft, such as aero-space-planes or winged bodies, therefore other possible entry trajectories.

References

- Bird, G.A. (1998), *Molecular Gas Dynamics and Direct Simulation Monte Carlo*, Clarendon Press, Oxford, U.K.
- Bird, G.A. (1999), *The DS2G Program User's Guide, Version 3.2*, G.A.B. Consulting Pty Ltd, Killara, Australia.

- Bird, G.A. (2005), *The DS2V Program User's Guide, Version 3.3*, G.A.B. Consulting Pty Ltd, Sydney, Australia.
- Bird, G.A. (2006), "Sophisticated versus simple DSMC", *Proceedings of the 25th International Symposium on Rarefied Gas Dynamics (RGD25)*, Saint Petersburg, Russia, July.
- Bird, G.A. (2008), *The DS2V Program User's Guide, Version 4.5*, G.A.B. Consulting Pty Ltd, Sydney, Australia.
- Bird, G.A. (2013), *The DSMC Method, Version 1.1*, Amazon, ISBN 9781492112907, Charleston, South Carolina, U.S.A.
- Bird, G.A., Gallis, M.A., Torczynski, J.R. and Rader, D.J. (2009), "Accuracy and efficiency of the sophisticated direct simulation Monte Carlo algorithm for simulating non-continuum gas flows", *Phys. Fluids*, **21**(1). <https://doi.org/10.1063/1.3067865>.
- Braun, R.D. and Manning, R.M. (2006), "Mars exploration entry, descent and landing challenges", *Proceedings of the 2006 IEEE Aerospace Conference*, Big Sky, Montana, U.S.A., March.
- Candler, G.V. and Boyd, I.D. (1994), "A multiple translational temperature gas dynamics model", *Phys. Fluids*, **6**(11), 3776-3786.
- Gallis, M.A., Torczynski, J.R., Rader, D.J. and Bird, G.A. (2009), "Accuracy and efficiency of the sophisticated direct simulation Monte Carlo algorithm for simulating non-continuum gas flows", *J. Comput. Phys.*, **228**(12), 4532-4548. <https://doi.org/10.1016/j.jcp.2009.03.021>.
- Gao, S., Habashi, W.G., Isola, D., Baruzzi, G.S., Fossati, M. and Uribarri, L. (2018a), "An edge-based Galerkin formulation for thermal non-equilibrium flows", *Proceedings of the 56th AIAA Aerospace Sciences Meeting*, Kissimmee, Florida, U.S.A., January.
- Gao, S., Seguin, J., Habashi, W.G., Isola, D. and Baruzzi, G.S. (2018b), "A finite solver for hypersonic flows in thermo-chemical non-equilibrium", *Proceedings of the 26th Annual Conference of the Computational Fluid Dynamics Society of Canada*, Winnipeg, Canada, June.
- Gao, S., Seguin, J., Habashi, W.G., Isola, D. and Baruzzi, G.S. (2019), "A finite solver for hypersonic flows in thermo-chemical non-equilibrium, Part II", *Int. J. Numer. Meth. Heat Fluid Flow*, **29**(9), 3148-3168. <https://doi.org/10.1108/HFF-12-2018-0725>.
- Justus, C.G. and Johnson, D.L. (2001), *Mars Global Reference Atmospheric Model 2001 (Mars-GRAM 2001) User Guide*, NASA TM 2001-210961.
- Moss, J.N. (1995), "Rarefied flows of planetary entry capsules", AGARD-R-808, 95-129, Special Course on "Capsule aerothermodynamics", Rhode-Saint-Genève, Belgium.
- NASA Glenn Research Center, Mars Atmosphere Model (1996), <https://www.grc.nasa.gov/WWW/K-12/airplane/atmosmre.html>.
- Pham Van-Diep, G., Erwin, D. and Muntz, E.P. (1989), "Nonequilibrium molecular motion in a hypersonic shock wave", *Science*, **245**(4918), 624-626. <https://doi.org/10.1126/science.245.4918.624>.
- Seguin, J., Habashi, W.G., Isola, D., Baruzzi, G.S. and Fossati, M. (2018), "Decoupled finite-element approach for high-Mach flows with finite-rate chemistry", *Proceedings of the 56th AIAA Aerospace Sciences Meeting*, Kissimmee, Florida, U.S.A., January.
- Shen, C. (2005), *Rarefied Gas Dynamic: Fundamentals, Simulations and Micro Flows*, Springer-Verlag, Berlin, Germany.
- Vallerani, E. (1973), "A review of supersonic sphere drag from the continuum to the free molecular flow regime", AGARD CPP 124, 1-15.
- Zuppari, G. (2004), "Evaluating anisotropy and thermodynamic non-equilibrium in hypersonic transitional regime", *Proceedings of the 24th International Symposium on Rarefied Gas Dynamics (RGD24)*, Monopoli, Italy, July.
- Zuppari, G. (2019a), "Influence of the Mars atmosphere model on aerodynamics of an entry capsule", *Adv. Aircraft Spacecraft Sci.*, **6**(3), 239-256. <https://doi.org/10.12989/aas.2019.6.3.239>.
- Zuppari, G. (2019b), "Influence of the Mars atmosphere model on 3-D aerodynamics of an entry capsule", *Proceedings of the Direct Simulation Monte Carlo Workshop DSMC19*, Santa Fe, New Mexico, U.S.A., September.
- Zuppari, G. (2020), "Influence of the Mars atmosphere model on aerodynamics of an entry capsule: Part

II”, *Adv. Aircraft Spacecraft Sci.*, 7(3), 229-249. <https://doi.org/10.12989/aas.2020.7.3.229>.
Zuppari, G. and Savino, R. (2015), “DSMC aero-thermo-dynamic analysis of a deployable capsule for Mars atmosphere entry”, *Proceedings of the Direct Simulation Monte Carlo Workshop DSMC15*, Kauai, Hawaii, U.S.A.

EC